NATIONAL ENERGY TECHNOLOGY LABORATORY
OIL & GAS

DOE Award No.: DE-FE0028973

Quarterly Research Performance Progress Report

(Period Ending 12/31/2017)

Advanced Simulation and Experiments of Strongly Coupled Geomechanics and Flow for Gas Hydrate Deposits: Validation and Field Application

Project Period (10/01/2016 to 09/30/2019)

Submitted by:
Jihoon Kim
Jihoon Kim
Signature

The Harold Vance Department of Petroleum Engineering,
College of Engineering
Texas A&M University
407K Richardson Building
3116 College Station TX, 77843-3136
Email: jihoon.kim@tamu.edu
Phone number: (979) 845-2205

Prepared for:
United States Department of Energy
National Energy Technology Laboratory

December 31, 2017

U.S. DEPARTMENT OF ENERGY | NATIONAL ENERGY TECHNOLOGY LABORATORY

Office of Fossil Energy

DISCLAIMER

TABLE OF CONTENTS

ACCOMPLISHMENTS

Objectives of the project

The objectives of the proposed research are (1) to investigate geomechanical responses induced by depressurization experimentally and numerically; (2) to enhance the current numerical simulation technology in order to simulate complex physically coupled processes by depressurization and (3) to perform in-depth numerical analyses of two selected potential production test sites: one based on the deposits observed at the Ulleung basin UBGH2-6 site; and the other based on well-characterized accumulations from the westend Prudhoe Bay. To these ends, the recipient will have the following specific objectives:

1). Information obtained from multi-scale experiments previously conducted at the recipient's research partner (the Korean Institute of Geoscience and Mineral Resources (KIGAM)) that were designed to represent the most promising known Ulleung Basin gas hydrate deposit as drilled at site UBGH2-6 will be evaluated (Task 2). These findings will be further tested by new experimental studies at Lawrence Berkeley National Laboratory (LBNL) and Texas A&M (TAMU) (Task 3) that are designed capture complex coupled physical processes between flow and geomechanics, such as sand production, capillarity, and formation of secondary hydrates. The findings of Tasks 2 and 3 will be used to further improve numerical codes.

2) Develop (in Tasks 4 through 6) an advanced coupled geomechanics and non-isothermal flow simulator ($T+M^{AM}$) to account for large deformation and strong capillarity. This new code will be validated using data from the literature, from previous work by the project team, and with the results of the proposed experimental studies. The developed simulator will be applied to both Ulleung Basin and Prudhoe Bay sites, effectively addressing complex geomechanical and petrophysical changes induced by depressurization (e.g., frost-heave, strong capillarity, cryo-suction, induced fracturing, and dynamic permeability).

Accomplished

The plan of the project timeline and tasks is shown in Table 1, and the activities and achievements during the fourth quarter of 2017 are listed as follows along with Table 2.

Task 1: Project management and planning

The fourth quarterly report was submitted to NETL at October 23, 2017. KIGAM has been working on Subtask 2.2 and 2.3. We have also made significant progress on Task 3 during this period. Specifically, Subtask 3.1 is completed, Subtask 3.2 is initiated, and Subtask 3.5 is almost completed. Because Subtask 2.1 was completed in the previous quarter, TAMU has been working on the data analysis related to Subtasks 4.1 and 5.2. The specific status of the milestones is shown in Table 2. Specific achievements during this period are as follows.

Task 2: Review and evaluation of experimental data of gas hydrate at various scales for gas production of Ulleung Basin

Subtask 2.1 Evaluation of Gas hydrate depressurization experiment of 1-m scale

This task is completed.

Subtask 2.2 Evaluation of Gas hydrate depressurization experiment of 10-m scale

We have been reviewing the processes and results of this experiment. In this report, we describe the experimental procedure, condition, and depressurization, continuing the description of the experimental settings shown in the previous quarterly report.

Experimental procedure: The system temperature is maintained at around 11^{o}C, the system is pressurized by methane injection, and then cooled to a given temperature. An abrupt decrease in the fluid pressure indicates hydrate formation. The depressurization is carried out to dissociate the hydrate-bearing sedimentary sample. By controlling the back pressure regulator, the fluid pressure of the sample is decreased from the stabilized pressure during hydrate formation to a designated pressure, which is lower than the equilibrium pressure. The pressure, temperature, and volume of the gas and water produced are recorded throughout the experimental process.

Experimental condition: The porosity of the prepared sample was 47.7%, and the absolute permeability was approximately 10.5 darcies ((μm)2). The average particle size was approximately 150 μm. Hydrates were formed in almost the same conditions; the initial pressure, formation temperature, and the initial water saturation were approximately 7.8 MPa, 1.0^{o}C, and 32.1%, respectively. The equilibrium pressure corresponding to the given temperature was approximately 2.90 MPa.

Depressurization test: Four depressurization tests were conducted by decreasing system pressure down to 10 (DP 10%), 20 (DP 20%), 30 (DP 30%), and 40% (DP 40%) against the equilibrium pressure of methane hydrate at a constant temperature condition. The data of the pressure, temperature, and gas production behavior over the elapsed time are being analyzed during the dissociation process.

Subtask 2.3 Evaluation of Gas hydrate depressurization experiment of 1.5-m scale system in 3D

We have initiated this task by reviewing the procedure of this experiment. To overcome the limitations in small scale experimental apparatus, such as cm-scale and 1D m-scale, we developed 3D meter-scale high pressure cell, and the system is composed of 4 major modules, which are 3D meter-scale high pressure cell, fluid control unit, data acquisition unit, and temperature control unit to simulate gas hydrate production in sediment specimens. Figure 1 shows a schematic diagram of 3D meter-scale GH production system.

The 3D meter-scale high pressure cell made of 316 stainless steel was constructed with the working pressure of 20 MPa in order to simulate a hydrate reservoir. The dimensions of sediment specimens are 1 m of the diameter and 1 m of the length. Five K-type thermocouples for the temperature measurement are equipped in every 20 cm from the bottom of the cell. Twenty pressure transducers are equipped in two places on the edge of cylindrical cell with 10 cm interval in the vertical direction. Custom-made electrodes are also equipped in every 10cm in the vertical direction for resistance measurement. A coolant circulation jacket was installed outside the high-pressure cell for direct temperature control of the cell. A CCD camera and a laser displacement sensor were installed at the top of the high pressure cell lid to observe sediment deformation. The fluid control system used mass flow controllers and a circulation pump for the injection and circulation of gas and water. Specifically, two autoclaves were installed to provide methane-dissolved water for gas hydrate formation. All of the above equipment is located in a large environmental chamber, which controls the temperature in the 0-25 degree range. Data acquisition system has been constructed for real time storage and processing of experimental data such as temperature, pressure, volume of production fluid, internal image of high pressure cell, and control of various measurement equipment obtained during depressurization production test.

Subtask 2.4 Evaluation of gas hydrate production experiment of the centimeter-scale system

This task is completed.

Task 3: Laboratory Experiments for Numerical Model Verification

To provide experimental data for numerical model verification, two types of tests were proposed. In the first tests described in Subtask 3.1, geomechanical changes resulting from effective stress changes during depressurization were examined. In the second set of tests described in Subtask 3.2, sand production during depressurization will be allowed. In the third test described in Subtask 3.3, measurement of capillary pressure during hydrate formation and secondary hydrate formation will be attempted.

Subtask 3.1: Geomechanical changes from effective stress changes during dissociation

Methane hydrate was formed in the porespace of a fine sand sample in an elastomer sleeve in an X-ray transparent pressure vessel. The sample was subjected to an initial effective stress. Hydrate was formed in the sand, and the sample resaturated with water. Methane was produced from the hydrate by depressurization which increased effective stress. Sample changes were monitored using X-ray CT and confining fluid volume changes. Sand production was prohibited by disallowing sand flow in the tubes by means of a plastic filter. Results in Figure 1 show a cross section of the sample during depressurization. Confining stress was 900 psi so the sequence in Figure 1 represents an increase of effective stress from 200 to 400 psi. The hydrate dissociation resulted in the density decrease (purple color), so the dark region presented the hydrate dissociation. From these images, we can observed that the hydrate dissociation front moved from outside into the center. No significant sample volume change was observed although a confining pressure which exceed the pore pressure up to 400 Psi was applied to the sample.

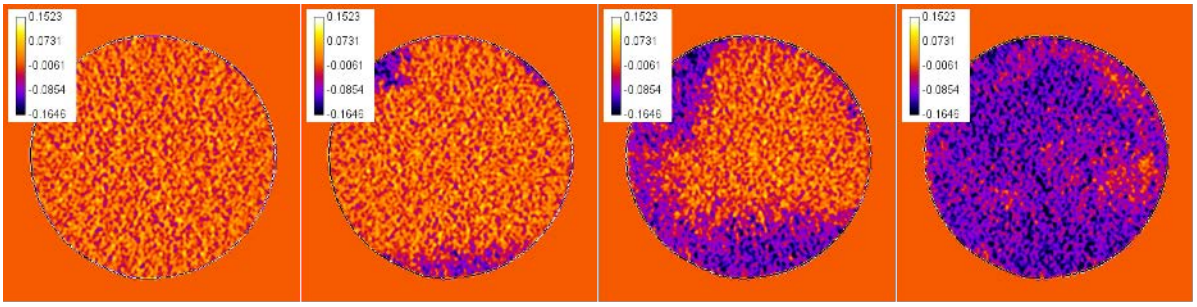

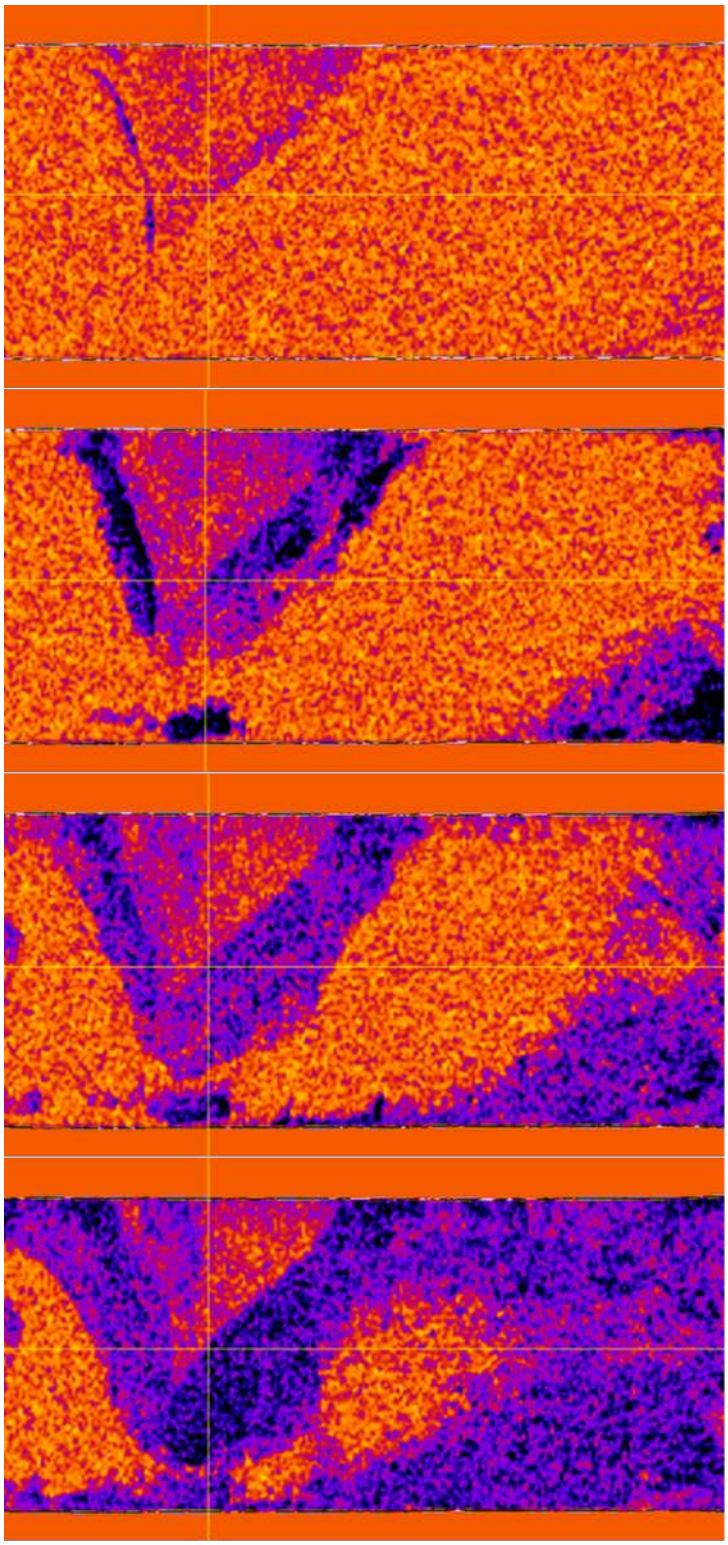

Figure 3.1a. From left to right, the density change with hydrate dissociation at the pressure of 700 psi, 600 Psi, 550 psi, 500 psi, respectively. b. Axial cross sectional slices of the CT scans. The arrow indicates the approximate location of the slice shown in a. The purple color indicates a reduction in density.

After completion of this experiment, simplified preliminary tests without hydrate formation were necessary to understand the baseline changes in geomechanics in the system due to flow and effective stress changes. The sample was reconstructed from partially saturated fine sand and the outlet plugged to prevent the flow of sand from the system. To attempt to better visualize minor shifting or movement of the sample, materials with different x-ray transparency were mixed with the sand placed in locations the sand column. Lower density areas were formed by mixing with diatomaceous earth (average particle size 100 um) and higher density areas with barite ($BaSO_4$). As with the hydrate formation test, the sample was placed in an X-ray transparent vessel and subjected to an initial effective stress. The effective stress was increased from an initial value of 100 psi to a value of 300 psi and changes to sample geometry were monitored. Subsequent to the effective stress changes, both gas and air flow were forced through the sample to model water and gas flow through the medium. Despite all the perturbations, only minor changes were seen in the sample over time. Figure 2 shows the initial sample, the sample after changes in effective stress and water flow. No overall volume changes were observed. Images represent a representative slice and cross sections the length of the sample.

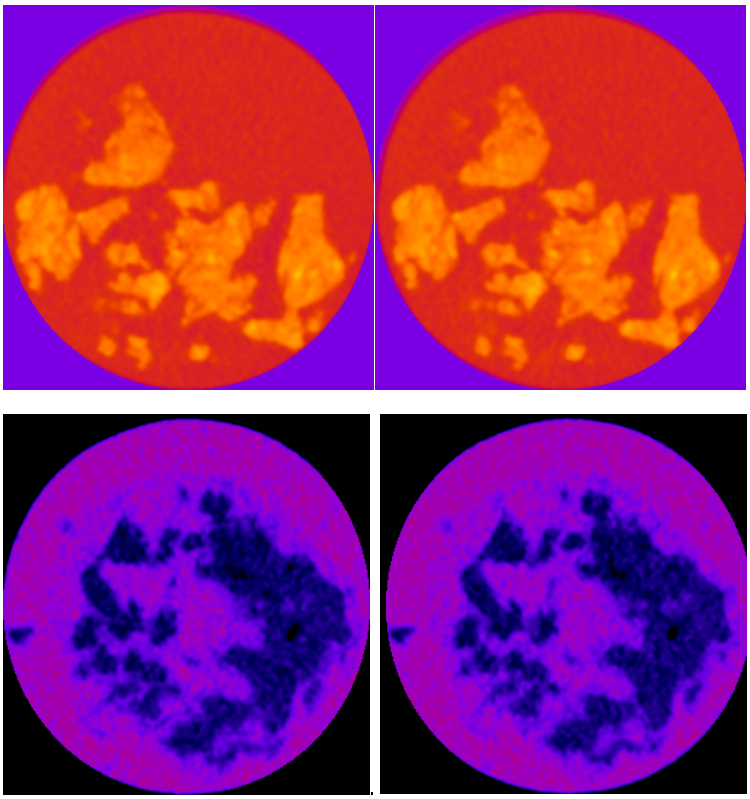

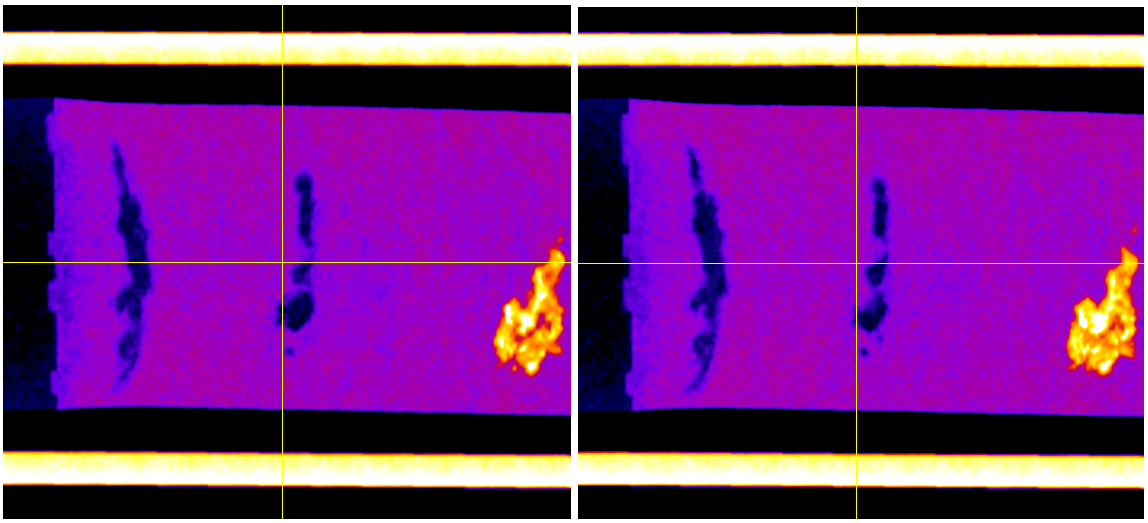

Figure 3.2. A slice of the sand sample through an area mixed with barite. (top) and mixed with diatomaceous earth (middle) and cross section through the sample (bottom) before and after completion of the test. Very little to no change was observed.

Subtask 3.2 Geomechanical changes from effective stress changes during dissociation – sand

Production

We have initiated this task. The same setup and general concept as used in Subtask 3.1 was used, however the plug preventing sand flow was removed and a sand trap was assembled so that flowing sand is not allowed to ruin experimental equipment. Initial pre-tests were performed in hydrate-free systems to examine the direct effect of effective stress on the medium while water is flowing. Initially we used 1/8 in tubing, but the flow was limited by the inner diameter of the tubing, so the tubing was increased to ¼ inch. Two configurations were tried, one with the outlet at the endcap and one with the outlet near the center of the samples (Figure 3). Both show flow of sand and deformation of the sample. After set up, the sample was initially exposed to increasing effective stress followed by a set confining pressure with increasing flow. The majority of the sand movement occurs during flow, not confining pressure changes.

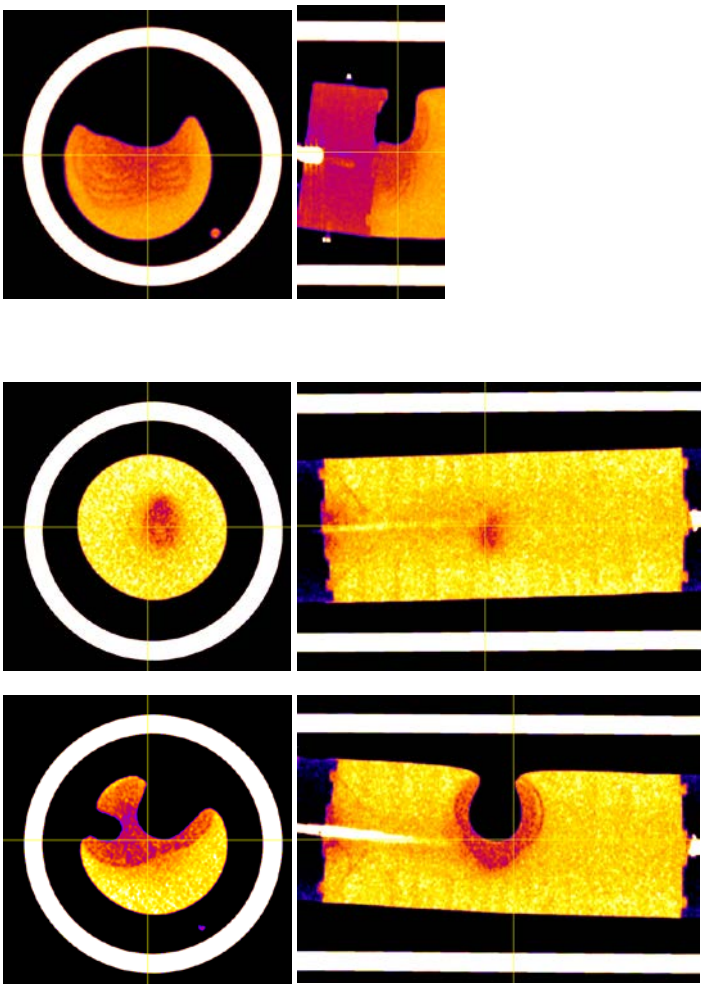

Figure 3.3. Top shows flow of sand from sample when outlet is located at the end of the sample. Middle and bottom show flow of sand from sample when outlet is located mid-sample. Middle is change observed due to a 300 psi increase in effective stress. Bottom is change in sample due to flow at 2 mL/min.

Subtask 3.3 Geomechanical changes resulting from secondary hydrate and capillary pressure changes

Not initiated (future year tasks)

Subtask 3.4 Construction of the Relative Permeability Data in Presence of Hydrate

Not initiated (future year tasks)

Subtask 3.5 Identification of Hysteresis in Hydrate Stability

Continuing the previous work, we are close to complete this task. Specific achievement is as follows. Between this report and the last report there was maintenance issues with the thermal chamber that is used for the experiments in TAMU. The maintenance has been completed and good results have been observed in the subsequent runs. Following the cooling measurements and history-matching study using simulation included the last progress report, we developed a series of cooling and heating cycles to investigate the hysteresis in the secondary hydrate formation in the water and gas saturated sand pack. In this progress report, we would like to go over these new results.

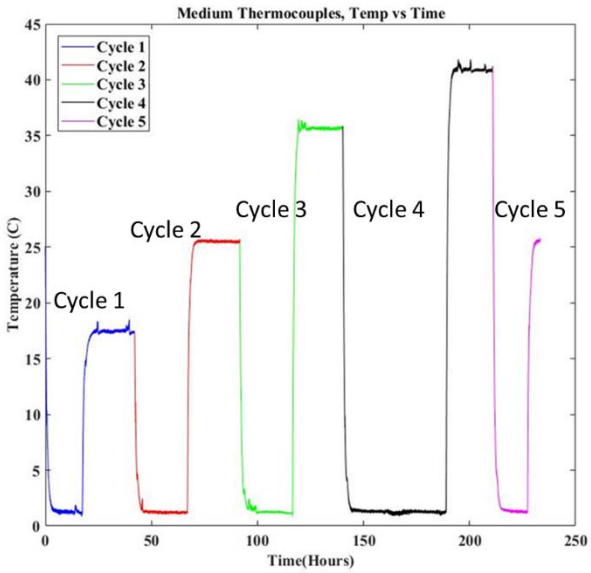

Figure 3.4: Thermal cycles experienced by the water-gas saturated sand pack thermocouple

In Figure 3.4 we show the cycles created using the thermal chamber. While there are not large differences seen here, each cycle shows a temperature spike when the hydrate forms inside the sand pack. The reason for multiple cycles with different melting temperatures is to identify and understand the secondary hydrate formation behavior. If there is hysteresis, the secondary hydrate formation should develop at a higher temperature in the new cycle depending on the melting temperature applied in the previous cycle. Further explanation will be given in the following pages during the analysis of the pressure versus temperature changes recorded for each thermal cycle.

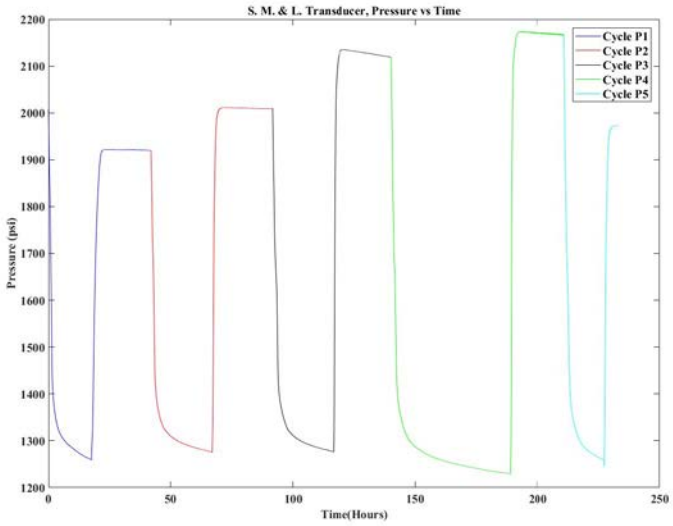

Figure 3.5: Pressure changes in the sand pack measured during the thermal cycles shown in Figure 3.4

In Figure 3.5 the pressure transients are shown for each thermal cycle. Notice that recorded pressure is much smoother relative to the temperature. This is expected because pressure change is diffusive and should be continuous. In other words, it should not be affected by the local perturbations in the regions of high heat transfer rate. Referring to the earlier figure in our previous report, we should note that the pressure is recorded at the top of the cylinder, whereas the temperature is recorded at three different locations in the sand pack. In this report, we show the recorded pressure-temperature profiles using the middle thermocouple which is radially located at the central portion of the tube. The other thermocouples give similar results, although the diagrams look somewhat noisier due to their location near the container wall.

Table 3.1 shows the melting and cooling temperatures introduced to the sand pack using the thermal chamber and pressures recorded in the sand pack. Note that the cooling temperature inside the chamber is always kept the same at 1C whereas the melting temperature for the secondary hydrate formations vary between 17-40C.

Table 3.1: Temperature cycles and their properties

Cycle	Melting Temp. (C)	Minimum Cooling. Temp. (C)	Pressure (psi)	Pressure at the Temp. spike (psi)
Cycle 1	N/A	1	2008	1787
Cycle 2	17	1	1922	1783
Cycle 3	25	1	2011	1833

Cycle 4	35	1	2119	1759
Cycle 5	40	1	2170	1745

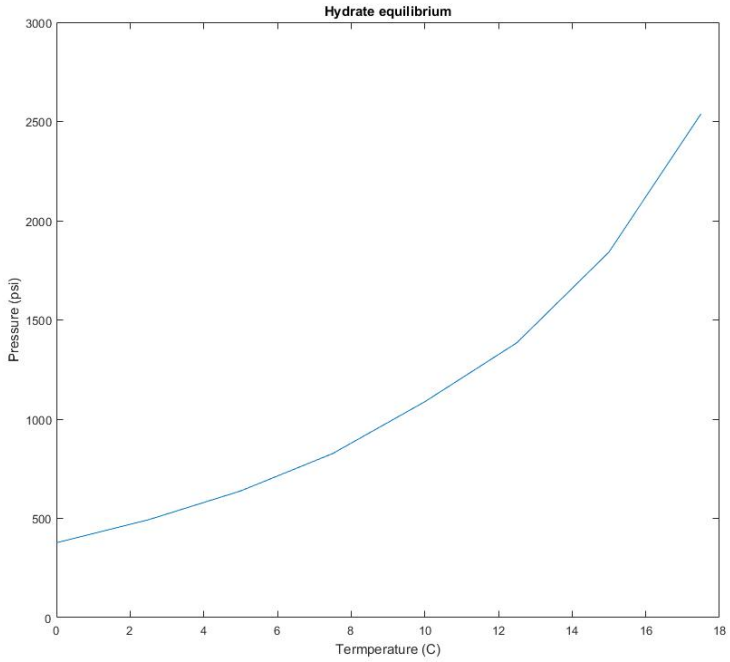

Figure 3.6: Methane hydrate equilibrium line on the pressure-temperature diagram

To ensure that hydrate has formed in the water-gas saturated sand pack, the pressure and temperature must be within the region above the line shown in Figure 3.6. The pressure and temperature point at which methane hydrate starts forming, however, is not necessarily the same as the hydrate equilibrium line. This sub-cooling effect will be explained further in the upcoming pages using the hydrate cycles.

Figure 3.7 shows the distribution of the water and methane gas in the sand pack during the application of the thermal cycles. Clearly, the two fluids are not homogeneously distributed. Water is introduced into the sand pack from the bottom of the apparatus and it occupied the lower 1/4 volume of the sand pack under the equilibrium conditions. Whereas gas is introduced very slowly from the top so that gas does not channel through the water phase. We would like to point that the middle thermocouple is located nearby the water-gas interface whereas the other thermocouples are located only in the water phase and gas phase. During the hydrate formation, we observed that the long thermocouple located in the water region does not experience temperature increase characteristic of the exothermic crystallization process and, therefore, we think that no gas exists around the long thermocouple and no hydrate forms. But the short thermocouple experience crystallization even though it is further away from the interface. This indicates to us that water reaches up to the region in vapor phase and the crystals may form at the surfaces of the grains where molecules of methane and water meet.

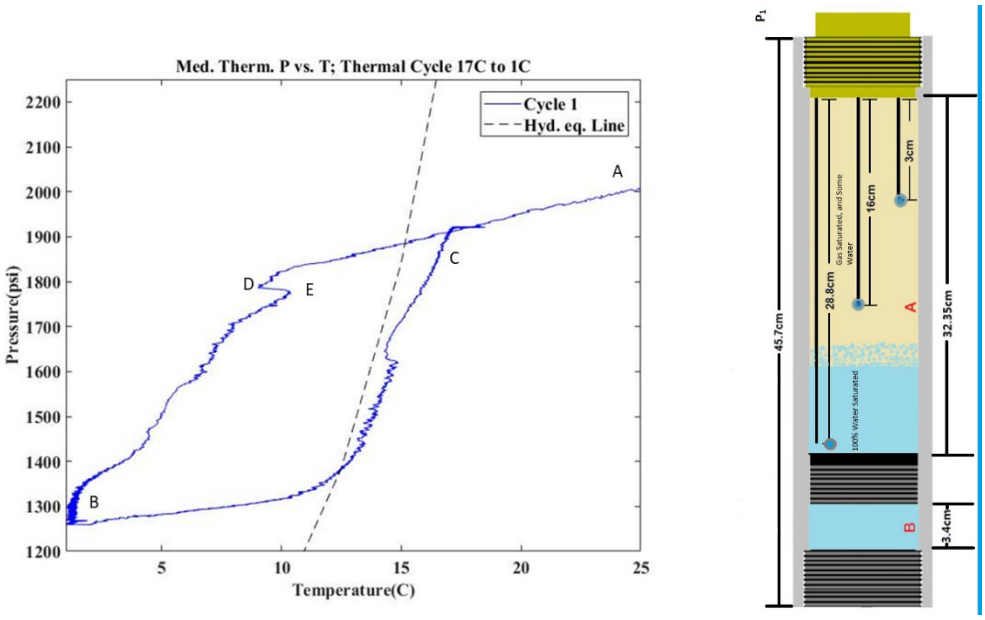

Figure 3.7: Pressure-temperature diagram during Cycle 1. Temperature is recorded using the middle thermocouple. Right: Hydrate cell blue is water saturated for A, and blue for B is the pressure chamber.

In Figure 3.7 the pressure versus temperature changes inside the sand pack is shown during the Cycle 1. Remember that in this cycle the temperature follows: 25C→1C→17C. Point A to B represents the system cooling from 25 to 1C. B to C is the system heating up to 17C. On this diagram the turning points D represents the initiation of the hydrate formation. Point D is of interest to our study because it shows the pressure and temperature point at which significant hydrate starts forming. As a consequence of this, the thermocouple records a significant increase in temperature during the cooling. Point E is the maximum hydrate production rate observed on the diagram. The horizontal distance from Point D to the equilibrium line is called in the literature the sub-cooling. When the hydrate is forming, the system loses gas and water so that the pressure continues to drop. On the diagram in between points E and B the pressure decline is much severe compared to pressure change with temperature only (in between points A and D). This is indicating that the hydrate formation continues between E and B.

The purpose of these experiments in our project using the various cycles is to classify where (at what pressure and what temperature) on the diagram the hydrate starts forming and at what time. When a sealed system is thermally cycled, if the system is reversible like the pendulum, one would expect to get similar results regardless of the melting temperature, since methane and water masses have not changed in the sand pack, and the melting temperature is always above the dissociation line. But let us look at the response of the system closely when the 2nd cycle and 3rd cycle is applied.

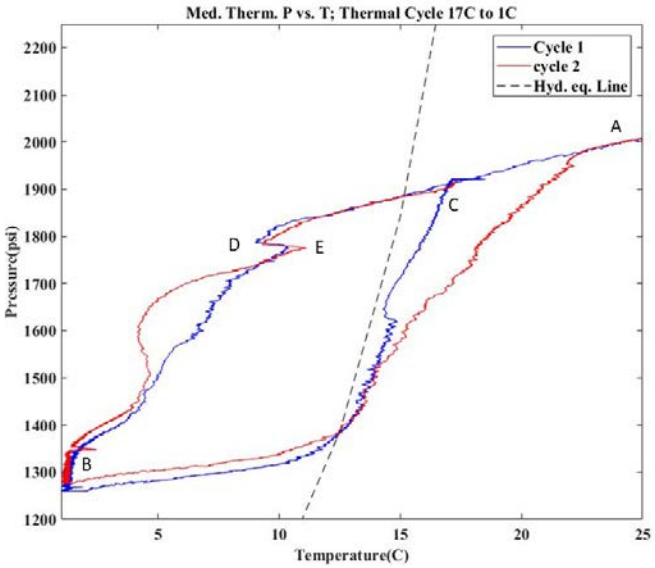

Figure 3.8: Thermal Cycle 2 compared to Cycle 1.

The red line in Figure 3.8 is the response of the system to Cycle 2 when the temperature follows 17C →1C→25C. It can be seen that point D is nearly the same as in Cycle 1 shown in blue, hitherto the reference line. The temperature is around 9C and the pressure is 1,785psi. The comparison of the two lines is important. In this cycle Point E has 3C increased temperature over that of the reference line. This means that even though the hydrates started forming at similar pressure-temperature point, the rate that they formed were higher in the case of Cycle 2.

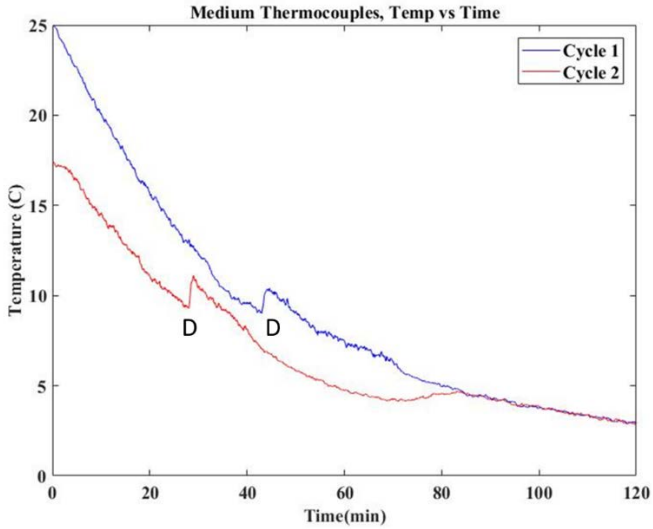

Figure 3.9: Temperature versus time for Cycles 1 and 2.

In Figure 3.9 the formation time for Cycle 2 starts forming at 28 minutes compared to 42.6 minutes for the Cycle 1. Point D in Figure 3.9 is the same point D in Figure 3.8, thus correlating the time of hydrate formation to the temperature properties of the pressure versus temperature plots. This indicates that even though the differences between points D in Figure 3.8 are very similar for the cycles, the times for hydrate crystallization are quite different.

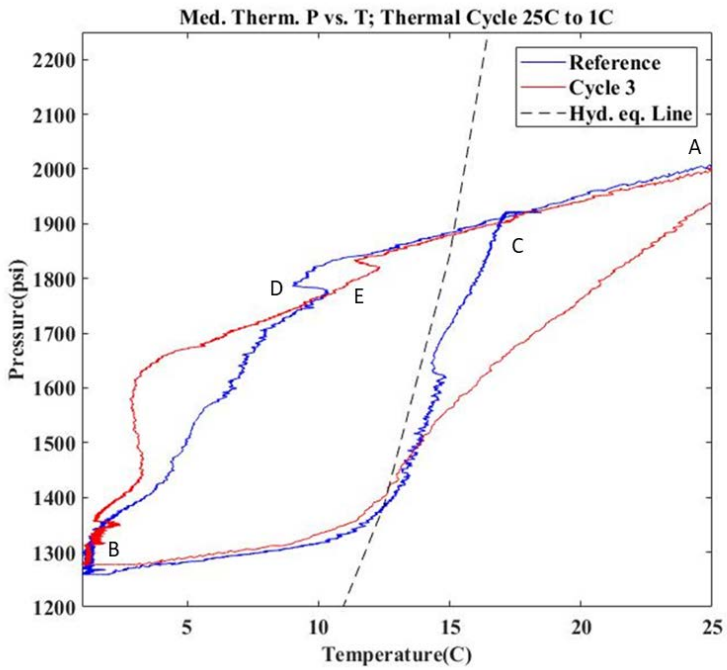

Figure 3.10: Thermal Cycle 3 compared to Cycle 1.

Figure 3.10 shows that Cycle 3 is largely different than the reference line. Cycle 3 has 25C→1C→35C. The result is interesting because both cycles have the same cooling paths 25C→1C. If no melting temperature effect at 25C, then one would expect identical cooling paths. However the results are indicating that Cycle 3 experiences hydrate formation at a point D much higher than that belongs to the Cycle 1. The hydrate in the case of Cycle 3 forms at a temperature 2.41C higher. Consequently, the sub-cooling is less for this cycle.

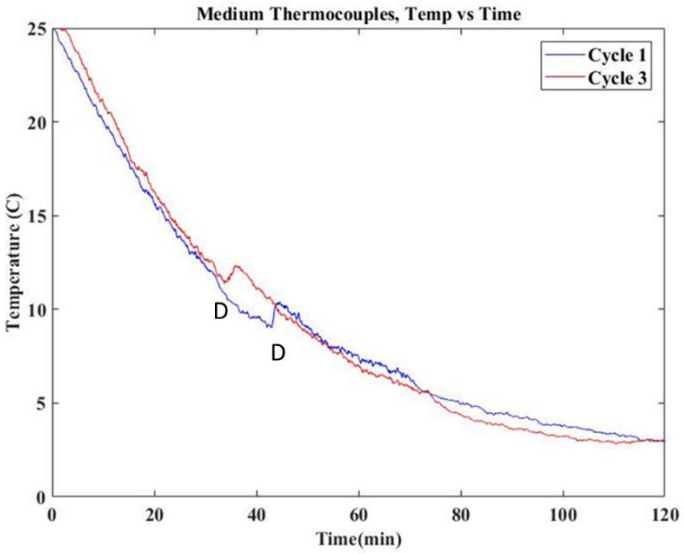

Figure 3.11: Temperature versus time for Cycles 1 and 3.

As in Figure 3.9, Figure 3.11 displays points D that are the same reference as point D in Figure 3.10. This indicates the time of formation of the methane hydrates for Cycle 1 and Cycle 3. The time for hydrate formation to start is 33.75 minutes for Cycle 3 and thus Cycle 3 forms 8.85 minutes earlier compared to the reference line. However, the difference in time while longer than that of Cycle 2, Cycle 3 has a higher initial temperature than the initial temperature of Cycle 2. The magnitude of the spike in temperature when the hydrate forms is the same which is indicating that the both cycles experienced similar heat transfer rates.

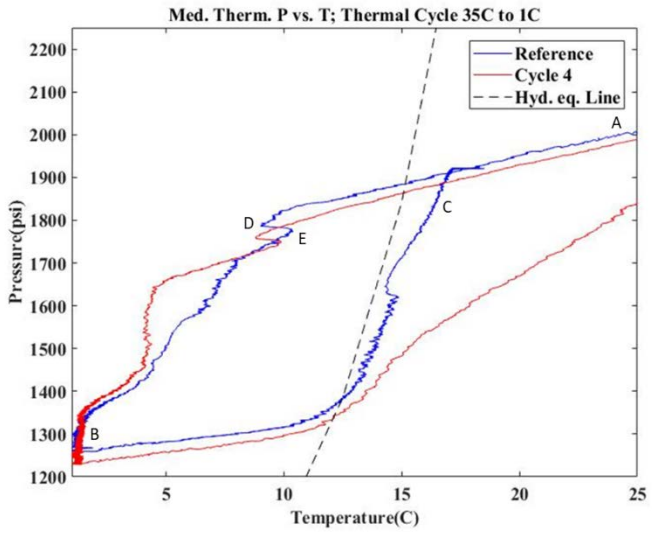

Figure 3.12: Thermal Cycle 4 compared to Cycle 1.

In Figure 3.12 Cycle 4 is discussed and compared to the reference line. Note that Cycle 4 experiences 35C→1C→40C. If one consider 40C as a high enough temperature to remove all the clusters of hydrates, then in this case one would expect the new results similar, if not the same, as the reference line. Figure 3.11 is showing that indeed the points D and E are very close in both cases. The only difference in these two curves is that the Cycle 4 experiences about 28 psi less pressure. This difference makes sense because Cycle cooling started at 25C whereas Cycle 4 at 35C. The similarity of the paths on the pressure-temperature indicating that the hysteresis is eliminated at this stage of melting. The time of hydrate formation for cycle 4 is much longer than that of cycle 1 because of the initial temperature and the required time to cool down to the hydrate equilibrium line is longer.

The final cycle experiences the highest melting temperature thus it should be the closest to the reference line, as follows.

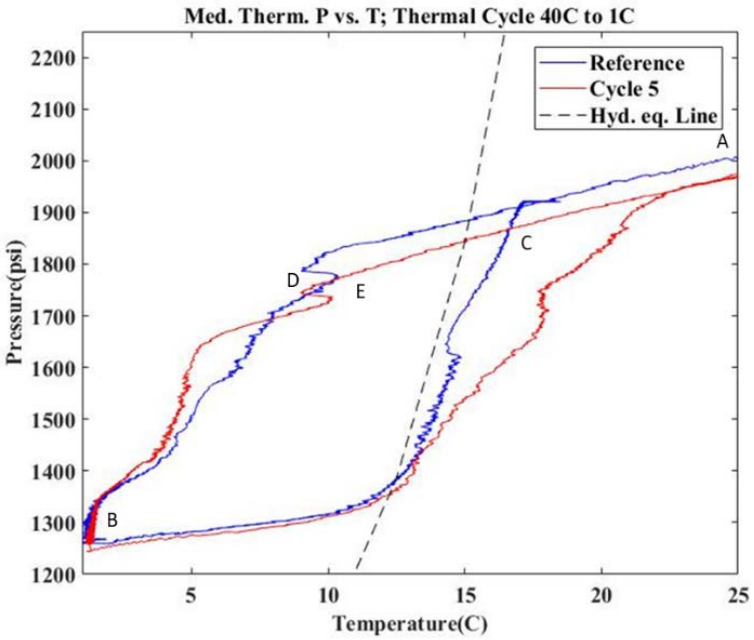

Figure 3.13: Thermal Cycle 5 compared to Cycle 1.

Cycle 5 experiences 40C→1C→25C. Figure 3.13 shows the expected results, that is the hydrate forms at exactly the same temperature of 9C. The temperatures recorded at points D and E for Cycle 5 and the reference line are so close that they are within the error of the thermocouples. As stated in the discussion of Figure 3.11 the small pressure difference experienced with Cycle 5 is that of the initial pressure from the melting stage of the last cycle. As in figure 3.12, the time taken to cool to the equilibrium line is longer than that of cycle 1 thus the time to formation of hydrate is longer.

Table 3.2: Experimental results

Cycle	Initial Temp. (C)	Point E Temp. (C)	Hydrate Formation Temperature (C)	Hydrate Formation time (min)	Point D Temperature (C)	Sub cooling (C)
Cycle 1	25	10.4	14.6	42.6	9	5.6
Cycle 2	17	11.1	14.7	28.08	9.3	5.4
Cycle 3	25	12.3	14.9	33.75	11.4	3.5
Cycle 4	35	9.9	14.5	60.5	8.8	5.7
Cycle 5	40	10.2	14.4	63.53	9	5.4

In conclusion, using our apparatus involving water-gas saturated sand pack, we showed the hydrate formation in the pressure-temperature diagrams. In addition, using thermal cycles, we show differences in sub-cooling depending on the melting temperatures applied to the hydrate. Thus, further work will be done using gas-sand and, water-sand, and the water-gas-sand systems and history-matching using simulation. The simulation-based history matching part of our work has already been started and will be reported in the next quarterly report.

Task 4: Incorporation of Laboratory Data into Numerical Simulation Model

Subtask 4.1 Inputs and Preliminary Scoping Calculations

Continuing the previous study, we have been performing processing the data from Subtask 2.1 for numerical simulation. From the experimental data, we identify non-uniform distribution of temperature (Figure 4.2) during gas production while the pressure is almost constant except for the case of SH=40% (Figure 4.1). Also, comparing the results between SH=30% and SH=40%, the two cumulative production are similar (Figure 4.3) while the vertical displacements are significantly different each other. We have these complex physical behavior due to different time scales as well as strong coupling among fluid flow, heat transfer, and geomechanics.

To prepare for the input data of numerical simulation, pressure (particularly for the cases of S_H=10%, S_H=20%, S_H=30%) can be taken as a minimum bottom hole pressure condition. Then, we can compare these experimental data with the numerical results of temperature, gas production, vertical displacement for validation of $T+M^{AM}$, Subtask 5.2.

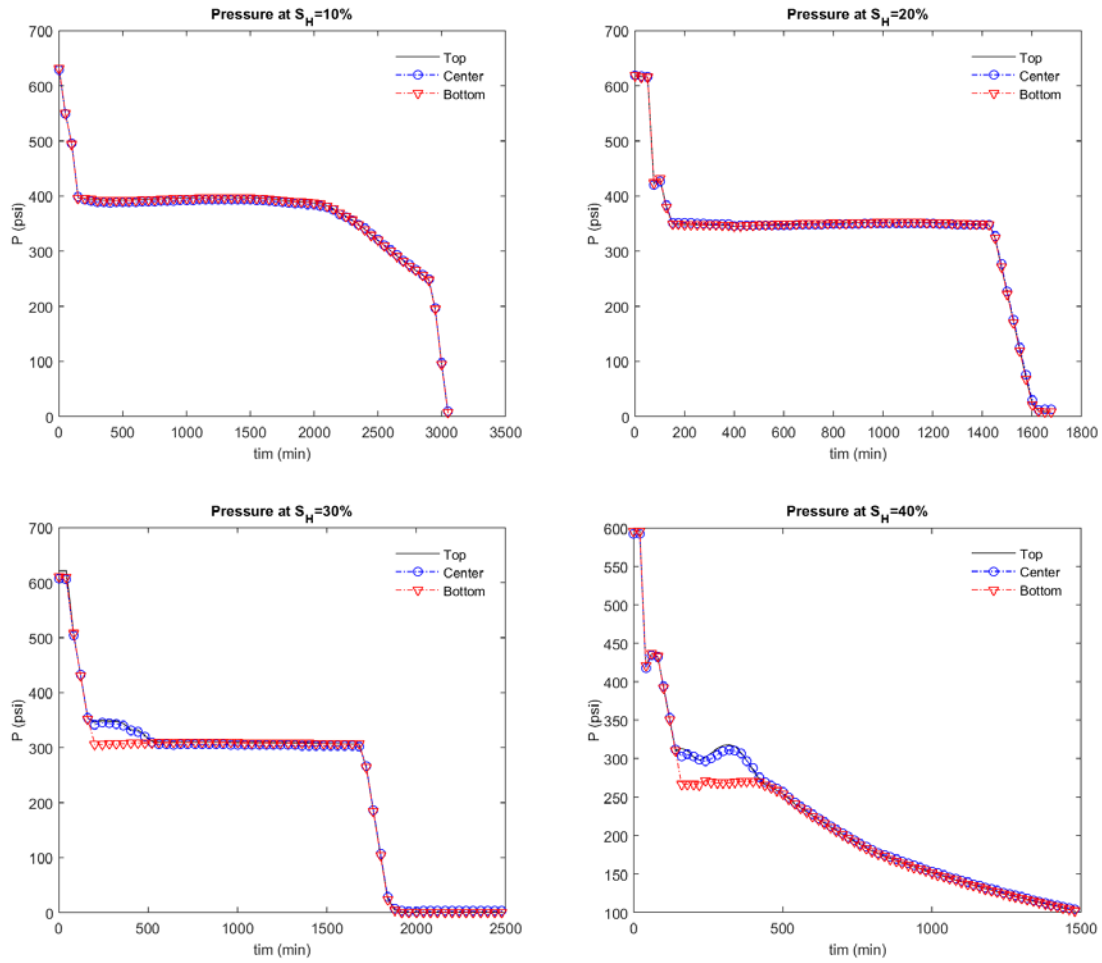

Figure 4.1 Evolution of pressure at the top, center, and bottom locations for the different initial hydrate saturations (S_H=10%, S_H=20%, S_H=30%, S_H=40%).

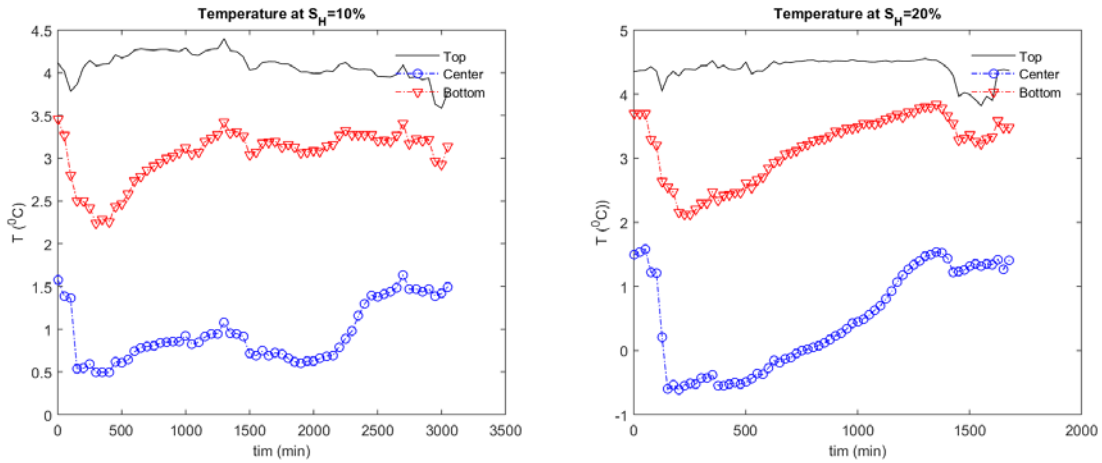

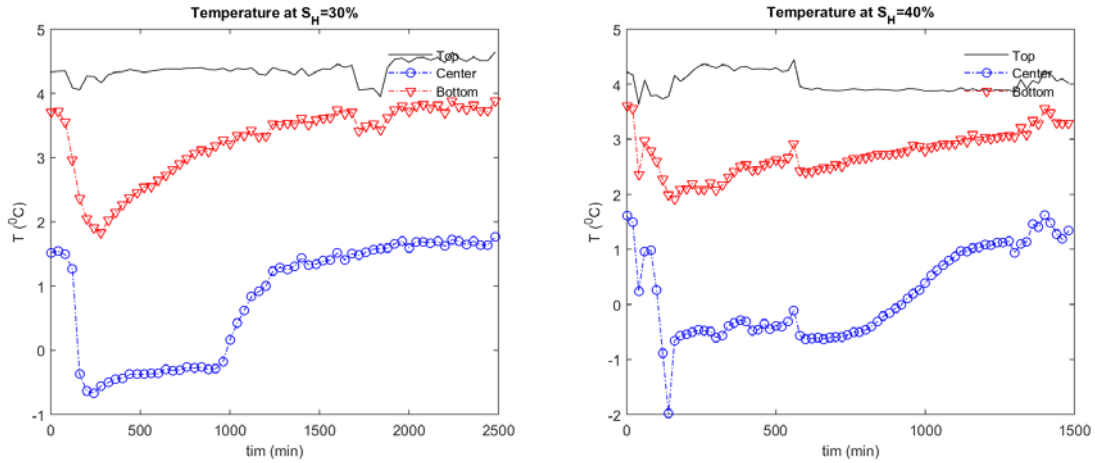

Figure 4.2 Evolution of temperature at the top, center, and bottom locations for the different initial hydrate saturations (S_H=10%, S_H=20%, S_H=30%, S_H=40%).

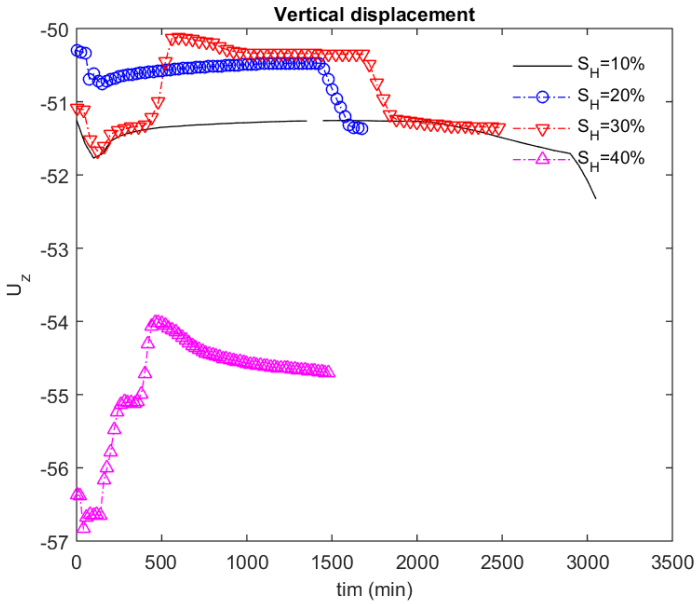

Figure 4.3 Evolution of vertical displacement at the top for different initial hydrate saturations (S_H=10%, S_H=20%, S_H=30%, S_H=40%).

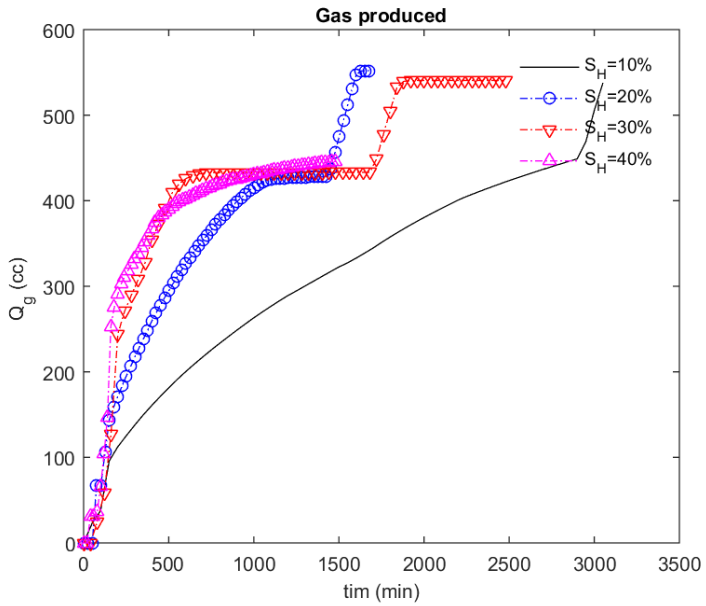

Figure 4.4 Evolution of gas production from different initial hydrate saturations (S_H=10%, S_H=20%, S_H=30%, S_H=40%).

Subtask 4.2 Determination of New Constitutive Relationships

Continuing the previous study, we keep updating TOUGH+Hydrate, modifying the subroutines of the hysteretic capillarity and relative permeability.

Subtask 4.3 Development of Geological Model

Not initiated (future research work)

Task 5: Modeling of coupled flow and geomechanics in gas hydrate deposits

Subtask 5.1 Development of a coupled flow and geomechanics simulator for large deformation

This task is completed.

Subtask 5.2 Validation with experimental tests of depressurization

After the progress of the previous quarter, no further progress was made during this period of September 30, 2017 ~ December 31, 2017. Because we have been analyzing the data of Subtask 2.1 (Subtask 4.1), we will be able to continue this task, next quarter.

Subtask 5.3 Modeling of sand production and plastic behavior

Not initiated (future task).

Subtask 5.4 Modeling of induced changes by formation of secondary hydrates: Frost-heave, strong capillarity, and induced fracturing

For modeling of the induced fracturing, we have been working on the Voronoi grid for flow, which can conform with the unstructured (triangle) finite element mesh for geomechanics. Currently, we have successfully generated and simulated the Voronoi grid for single phase flow, where its mesh file has the same format as TOUGH+Hydrate. At the next step, we will move to TOUGH+Hydrate with the Voronoi grid and/or the induced fracturing simulation of ROCMECH.

Subtasks 5.5 and 5.6 Field-scale simulation of PBU L106 and Ulleung Basin

No further progress was made during this period of September 30, 2017 ~ December 31, 2017.

Task 6: Simulation-Based Analysis of System Behavior at the Ignik-Sikumi and Ulleung Hydrate Deposits

We have trained thoroughly a TAMU student in the use and application of the Tough+Hydrate code. We are continuing simulations using the new axisymmetric geomechanical code.

PRODUCTS

One Ph.D student funded by this project (Yoon, Hyun Chul) graduated on December 15, 2017. This fund is acknowledged.

A paper titled ‘Spatial stability for the monolithic and sequential methods with various space discretizations in poroelasticity’ by Yoon and Kim has been accepted in International Journal for Numerical Methods in Engineering, which is currently in press. This fund is also acknowledged.

All parties of TAMU, LBNL, KIGAM have been participating in the 2nd International Gas Hydrate Code Comparison Study teleconference (IGHCCS2) held every two weeks online. Specifically, TAMU and LBNL gave talks on December 7, 2017. In the web-meeting, both TAMU and LBNL presented the capabilities of coupled flow-geomechanics codes owned by TAMU and LBNL, respectively.

BUDGETARY INFORMATION

Table 3 shows the information of the budget for this project and the expenditure up to 12/31/2017. We made the minor update of the expense of LBNL incurred during the previous quarter (2017 Q4).

Table 1 – Initial project timeline and milestones (Gantt Chart)

	FY17				FY18				FY19			
Quarter	Q1	Q2	Q3	Q4	Q1	Q2	Q3	Q4	Q1	Q2	Q3	Q4
Task 1.0. Project Management/Planning	A											
Task 2.0. Experimental study of gas hydrate in various scales for gas production of Ulleung Basin												
Subtask 2.1. Depressurization of 1 m scale in 1D				B								
Subtask 2.2 Depressurization of 10-m scale in 1D							C					
Subtask 2.3. Depressurization of 1.5-m scale in 3D										D		
Subtask 2.4. Revisit to the centimeter-scale system												
Task 3.0. Laboratory Experiments for Numerical Model Verification												
Subtask 3.1. Effective stress changes during dissociation				E								
Subtask 3.2. Sand production								F				
Subtask 33. Secondary hydrate and capillary pressure changes												G
Subtask 3.4. Relative Permeability Data												
Subtask 3.5. Hysteresis in Hydrate Stability												
Task 4.0. Incorporation of Laboratory Data into Numerical Simulation Model												
Subtask 4.1. Inputs and Preliminary Scoping Calculations									H			
Subtask 4.2. Determination of New Constitutive Relationships												
Subtask 4.3. Development of Geological Model												
Task 5.0. Modeling of coupled flow and geomechanics in gas hydrate deposits												
Subtask 5.1 Development of a coupled flow and geomechanics simulator for large deformation				I								
Subtask 5.2 Validation with experimental tests of depressurization										J		
Subtask 5.3 Modeling of sand production and plastic behavior								K				
Subtask 5.4 Frost-heave, strong capillarity, and induced fracturing												L
Subtask 5.5 Field-scale simulation of PBU L106												
Subtask 5.6 Field-wide simulation of Ulleung Basin												

Task 6.0. Simulation-Based Analysis of System Behavior at the Ignik-Sikumi and Ulleung Hydrate Deposits												**M**

Table 2. Milestones Status

Milestone	Description	Planned Completion	Actual Completion	Status / Comments
Task 1 Milestones				
Milestone A	Complete the kick-off meeting and revise the PMP	12/31/17	1/14/2017	Kickoff meeting held 11/22/17, revised PMP finalized 1/17/17
Task 2 Milestones				
Milestone B	Complete analysis of 1 m-scale experiment in 1D and validation of the cm-scale system (FY17, Q4)	9/30/2017		Completed.
Milestone C	Complete analysis of 10m-scale experiment in 1D	6/30/2018		
Milestone D	Complete analysis of 1.5m-scale experiment in 3D			
Task 3 Milestones				
Milestone E	Complete geomechanical changes from effective stress changes during dissociation and construction of the relative permeability data	9/30/2017		Completed
Milestone F	Complete geomechanical changes from effective stress changes during dissociation (sand production) and hysteresis in hydrate stability	9/30/2018		
Milestone G	Complete geomechanical changes resulting from secondary hydrate and capillary pressure changes	9/30/2019		
Task 4 Milestones				
Milestone H	Complete inputs and preliminary scoping calculations, determination of New Constitutive Relationships, development of Geological Model	12/31/2018		
Task 5 Milestones				
Milestone I	Complete development of a coupled flow and geomechanics simulator for large deformation, validation with experimental tests of Subtasks 2.1 and 2.4.	9/30/17		Completed.
Milestone J	Validation with experimental tests of Task 2 and 3	3/31/2019		
Milestone K	Complete modeling of sand production and plastic	9/30/2018		

	behavior, validation with experimental tests of Subtasks 2.2			
Milestone L	Complete field-scale simulation of the Ulleung Basin and PBU L106	3/31/2019		
Task 6 Milestones				
Milestone M	Complete Task 6	9/30/2019		

Table 3 Budget information

Baselinie Reporting Quarter	Budget Period 1							
	Q1		Q2		Q3		Q4	
	10/01/16-12/31/16		01/01/17-03/31/17		04/01/17-06/30/17		07/01/17-09/30/17	
	Q1	Cumulative Total	Q2	Cumulative Total	Q3	Cumulative Total	Q4	Cumulative Total
Baselinie Cost Plan								
Federal (TAMU)	$37,901	$37,901	$57,809	$95,711	$43,967	$139,678	$34,206	$173,884
Federal (LBNL)	$18,750	$18,750	$18,750	$37,500	$18,750	$56,250	$18,750	$75,000
Non-Federal Cost Share	$6,986	$6,986	$6,986	$13,972	$6,986	$20,958	$656,986	$677,944
Total Planned	$63,637	$63,637	$83,545	$147,183	$69,703	$216,886	$709,942	$926,828
Actual Incurred Cost								
Federal (TAMU)	$0	$0	$10,235	$10,235	$57,085	$67,321	$54,167	$121,488
Federal (LBNL)	$0	$0	$0	$0	$0	$0	$8,500	$8,500
Non-Federal Cost Share	$0	$0	$6,986	$6,986	$6,986	$13,972	$156,986	$170,958
Total incuured cost	$0	$0	$17,221	$17,221	$64,071	$81,293	$219,653	$300,946
Variance								
Federal (TAMU)	($37,901)	($37,901)	($47,574)	($85,475)	$13,118	($72,357)	$19,961	($52,396)
Federal (LBNL)	($18,750)	($18,750)	($18,750)	($37,500)	($18,750)	($56,250)	($10,250)	($66,500)
Non-Federal Cost Share	($6,986)	($6,986)	$0	($6,986)	$0	($6,986)	($500,000)	($506,986)
Total variance	($63,637)	($63,637)	($66,324)	($129,961)	($5,632)	($135,593)	($490,289)	($625,882)

Baselinie Reporting Quarter	Budget Period 2							
	Q1		Q2		Q3		Q4	
	10/01/17-12/31/17		01/01/18-03/31/18		04/01/18-06/30/18		07/01/18-09/30/18	
	Q1	Cumulative Total	Q2	Cumulative Total	Q3	Cumulative Total	Q4	Cumulative Total
Baselinie Cost Plan								
Federal (TAMU)	$42,481	$42,481	$35,307	$77,788	$46,367	$124,155	$39,908	$164,063
Federal (LBNL)	$18,750	$18,750	$18,750	$37,500	$18,750	$56,250	$18,750	$75,000
Non-Federal Cost Share	$6,986	$6,986	$6,986	$13,972	$6,986	$20,958	$6,986	$27,944
Total Planned	$68,217	$68,217	$61,043	$129,260	$72,103	$201,363	$65,644	$267,007
Actual Incurred Cost								
Federal (TAMU)	$35,832	$35,832						
Federal (LBNL)	$45,952	$45,952						
Non-Federal Cost Share	$6,986	$6,986						
Total incuured cost	$88,770	$88,770						
Variance								
Federal (TAMU)	($6,650)	($6,650)						
Federal (LBNL)	$27,202	$27,202						
Non-Federal Cost Share	$0	$0						
Total variance	$20,552	$20,552						

Baselinie Reporting Quarter	Budget Period 3							
	Q1		Q2		Q3		Q4	
	10/01/18-12/31/18		01/01/19-03/31/19		04/01/19-06/30/19		07/01/19-09/30/19	
	Q1	Cumulative Total	Q2	Cumulative Total	Q3	Cumulative Total	Q4	Cumulative Total
Baselinie Cost Plan								
Federal (TAMU)	$43,543	$43,543	$36,189	$79,733	$47,526	$127,259	$41,209	$168,468
Federal (LBNL)	$18,750	$18,750	$18,750	$37,500	$18,750	$56,250	$18,750	$75,000
Non-Federal Cost Share	$6,986	$6,986	$6,986	$13,972	$6,986	$20,958	$6,986	$27,944
Total Planned	$69,279	$69,279	$61,925	$131,205	$73,262	$204,467	$66,945	$271,412
Actual Incurred Cost								
Federal (TAMU)								
Federal (LBNL)								
Non-Federal Cost Share								
Total incuured cost								
Variance								
Federal (TAMU)								
Federal (LBNL)								
Non-Federal Cost Share								
Total variance								

National Energy Technology Laboratory

626 Cochrans Mill Road
P.O. Box 10940
Pittsburgh, PA 15236-0940

3610 Collins Ferry Road
P.O. Box 880
Morgantown, WV 26507-0880

13131 Dairy Ashford Road, Suite 225
Sugar Land, TX 77478

1450 Queen Avenue SW
Albany, OR 97321-2198

Arctic Energy Office
420 L Street, Suite 305
Anchorage, AK 99501

Visit the NETL website at:
www.netl.doe.gov

Customer Service Line:
1-800-553-7681

U.S. DEPARTMENT OF ENERGY | NATIONAL ENERGY TECHNOLOGY LABORATORY